Int J CARS
DOI 10.1007/s11548-015-1211-4

ORIGINAL ARTICLE

Design and performance evaluation of a master controller for endovascular catheterization

Jin Guo[1] · Shuxiang Guo[2,3] · Takashi Tamiya[4] · Hideyuki Hirata[2] · Hidenori Ishihara[2]

Received: 8 January 2015 / Accepted: 7 April 2015

Abstract
Purpose It is difficult to manipulate a flexible catheter to target a position within a patient's complicated and delicate vessels. However, few researchers focused on the controller designs with much consideration of the natural catheter manipulation skills obtained from manual catheterization. Also, the existing catheter motion measurement methods probably lead to the difficulties in designing the force feedback device. Additionally, the commercially available systems are too expensive which makes them cost prohibitive to most hospitals. This paper presents a simple and cost-effective master controller for endovascular catheterization that can allow the interventionalists to apply the conventional pull, push and twist of the catheter used in current practice.
Methods A catheter-sensing unit (used to measure the motion of the catheter) and a force feedback unit (used to provide a sense of resistance force) are both presented. A camera was used to allow a contactless measurement avoiding additional friction, and the force feedback in the axial direction was provided by the magnetic force generated between the permanent magnets and the powered coil.
Results Performance evaluation of the controller was evaluated by first conducting comparison experiments to quantify the accuracy of the catheter-sensing unit, and then conducting several experiments to evaluate the force feedback unit. From the experimental results, the minimum and the maximum errors of translational displacement were 0.003 mm (0.01 %) and 0.425 mm (1.06 %), respectively. The average error was 0.113 mm (0.28 %). In terms of rotational angles, the minimum and the maximum errors were 0.39° (0.33 %) and 7.2° (6 %), respectively. The average error was 3.61° (3.01 %). The force resolution was approximately 25 mN and a maximum current of 3A generated an approximately 1.5 N force.
Conclusion Based on analysis of requirements and state-of-the-art computer-assisted and robot-assisted training systems for endovascular catheterization, a new master controller with force feedback interface was proposed to maintain the natural endovascular catheterization skills of the interventionalists.

Keywords Endovascular catheterization · A force feedback device · Contactless measurement · Training · A master controller

✉ Jin Guo
s12d503@stmail.eng.kagawa-u.ac.jp

Shuxiang Guo
guo@eng.kagawa-u.ac.jp

1 Graduate School of Engineering, Kagawa University, Takamatsu, Kagawa, Japan

2 Intelligent Mechanical Systems Engineering Department, Kagawa University, Takamatsu, Kagawa, Japan

3 School of Life Science, Beijing Institute of Technology, Haidian District, Beijing, China

4 Department of Neurological Surgery, Faculty of Medicine, Kagawa University, Takamatsu, Kagawa, Japan

Introduction

Catheter-based endovascular interventional procedures have been extensively adopted for treatment and diagnosis of various vascular diseases. During the procedures, a flexible catheter having a pre-bent shape with a natural curvature at the tip is directed inside the patient's vascular structure, from the femoral artery to the target position, by manipulating the tail part of the catheter [1]. The gradually increasing success rate of catheter-based interventions, combined with less

Published online: 13 June 2015

blood loss and minimal damage to healthy tissue, has led to a significant growth in the number of procedures performed annually. However, it is still challenging work to position a catheter in a target vessel branch within the highly complicated and delicate vascular structure. The interventionalists have to carry out operations by imagining the spatial relationship between the catheter and its surrounding vessels based on their experience and feelings due to the lack of intuitive visual feedback [2,3]. Additionally, complicated vessel shapes and multi-contacts between the catheter and the blood vessel walls lead to significant deterioration in the feasibility and maneuverability of positioning the catheter [4]. The catheter manipulation skills of experienced interventionalists are therefore critical to the success of endovascular catheterization.

To afford novice interventionalists, the opportunity to learn basic catheter manipulation skills, robot-assisted and computer-assisted catheterization training methods are two promising approaches. Two commercially available endovascular simulators are the Procedicus Vascular Interventional System Trainer [5,6] (VIST, Mentice AB, Gothenburg, Sweden) and the Angio Mentor^{TM} [7,8] (Simbionix, Ltd., Cleveland, OH, U.S.), which allow novice interventionalists to conduct comprehensive, goal-oriented training during their education program before treating real patients including catheter/wire manipulating, stent deployment and angioplasty balloon inflation in the renal, carotid, aortoiliac and peripheral vascular structures [9]. The Sensei robotic navigation system [10,11] (Hansen Medical, Mountain View, Calif) and the Niobe magnetic navigation system [12,13] (Stereotaxis, St. Louis, Mo) are two typically commercial surgical robotic systems that have been used in endovascular interventional surgery with electromechanical bases and magnetically controlled mechanisms of action. They have been successfully used in different clinical applications including cardiac ablation and endovascular aneurysm repair [14]. However, there are several limitations to the application of these commercial products. The most obvious one is the expensive cost of the systems, which makes them inaccessible to most private centers [15–17]. Additionally, the catheters must be integrated with their custom interfaces and navigation systems to do the catheterization operations, which is not always possible.

In addition to the commercially available products, many research groups have studied endovascular interventional training systems. Cercenelli et al. [18,19] developed a novel telerobotic system to manipulate standard electrophysiology catheters. However, there is no force feedback device in their controller design. The loss of force feedback in robotic catheter systems can increase the risk of damage to the blood vessel walls. Fukuda et al. [20–22] at Nagoya University have developed a joystick as the controller of the master system with a haptic unit to handle the manipulators of the slave system. There are two joints in the design of the master controller, and each joint is connected to a motor with a wire mechanism. Another research group in [23] designed a master controller to simulate the conventional push, pull and rotate motion used in current practice. However, unlike the conventional endovascular catheterization, in which interventionalists manipulate an actual catheter directly using their hands, the employment of these master controllers replaces the catheter from the interventionalists' hand with the "handle part," which are made of metal materials with different size and material attributes from a real catheter, to carry out catheterization training operations. The loss of touching a real catheter unavoidably contaminates their intuitive and dexterous skills in the interventional radiology procedure. To achieve better training effects, Thakur et al. [24] developed a novel remote catheter navigation system to directly manipulate percutaneous transluminal catheters from a location far away from the patient while allowing the interventionalists to apply conventional insertion, extraction and rotation motion in the procedure. A similar design was presented by researchers in [25]. However, these research achievements have a common defect: To measure the motion of the input catheter, the catheter is needed to be clamped by the rollers coupled with encoders; to ensure the catheter does not slip in the apparatus, a force has to be applied to the rollers. This kind of design leads to difficulties in developing the force feedback device to provide the interventionalists with a sense of resistance force.

To address the need for providing a familiar and ergonomic setting for the interventionalists, we have designed a compact master controller capable of simultaneously measuring the radial and axial motion of the input catheter to provide force feedback while preserving the manual catheter manipulation skills which is operated by the interventionalists. A camera was used to allow contactless measurement that avoids additional friction while the force feedback in the axial direction was provided by the magnetic force generated between the permanent magnets and the powered coil.

Materials and methods

As researchers in [14] have pointed out, ideal catheterization training systems should be designed with consideration given to conventional catheter-handling skills used in a real endovascular interventional surgery. In this paper, we focused mainly on the design of a master controller to allow the interventionalists to employ an actual catheter, as the controller, to carry out training courses with force feedback in an ergonomic, compact and simple setting.

Overview of the proposed master controller

The proposed master controller consists of a catheter-sensing unit capable of measuring translational and rotational motions of the input catheter, a force feedback unit capable of providing a resistance force on the input catheter, and a control console that transmits information for the force feedback unit and the motors (shown in Fig. 1a).

A camera was fixed directly above the catheter (shown in Fig. 1b) to detect the feature points attached to the catheter. The translational displacement and rotational angles of the input catheter were calculated according to the movements of the feature points. Two catheter holders were used to make the catheter a straight line and as parallel as possible to the imaging plane of the camera. A series of repeated experiments were conducted to determine the relationship between the pixel units and the physical units. Thus, even though the catheter was slightly nonparallel to the imaging plane, the error can be reduced significantly by the relationship calibration. A bearing was fixed in the middle of the bearing holder between the low-friction slider and the coil plate. The catheter passes through the bearing with a grasper, which is employed to integrate the catheter with the coil plate. Four permanent magnets are arranged within the magnet's shell, which is anchored on the movement stage of a screw bearing actuated by a stepper motor. The coil plate is located inside the magnet's shell, in the middle position between two above magnets and two below magnets. To provide force feedback in the axial direction, the magnetic force was generated by the permanent magnets and the energized coil. When the interventionalists push or pull the catheter, the stepper motor controls the position of the magnet's shell keeping the magnet's shell relatively static to the coil plate according to the displacement of the catheter based on a position-control loop.

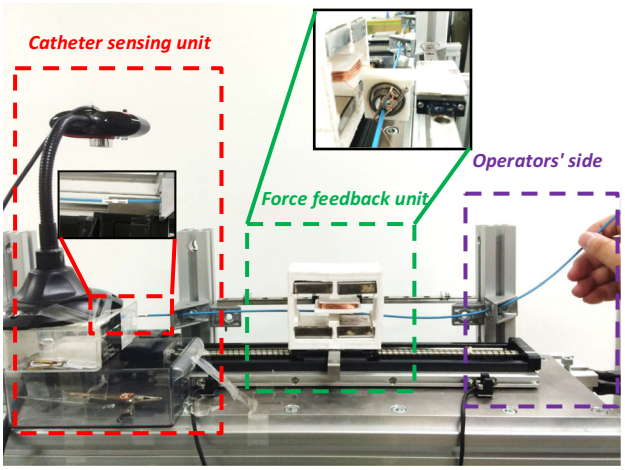

(a)

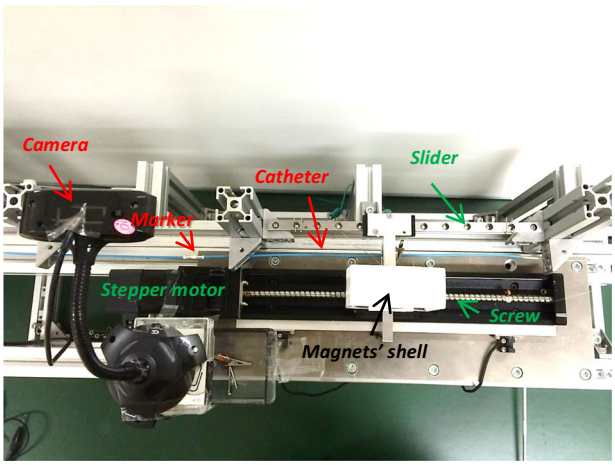

(b)

Fig. 1 Structure of the proposed new master controller. **a** The front view of the master controller. **b** The top view of the master controller

Catheter-sensing methods

To avoid additional friction and to allow the interventionalists to advance the catheter using push, pull and rotate techniques, a camera was employed to simultaneously measure the axial and radial motions of the input catheter.

Due to manufacturing reasons, an unavoidable problem of lens distortion occurred when using the camera to determine the catheter's position. In practice, two main distortions, radial distortions generated due to the shape of the lens and tangential distortions resulting from the assembly process of the camera as a whole, should be considered [26]. To obtain both the model of the camera's geometry and a distortion model of the lens, the process of camera calibration was performed based on Zhang's method [27]. This method is simple and based mainly on different nonparallel views of a planar pattern, such as a chessboard. The frames of a chessboard pattern were captured from a variety of angles and positions. The corners of the black and white squares were detected and used to calculate the exact locations of the corners on a sub-pixel accuracy level. A homograph matrix was identified based on a maximum-likelihood algorithm, and the camera's intrinsic parameters were separated from the perspective projection matrix under the assumption of no camera distortion. The extrinsic parameters for each image of the chessboard pattern were then determined to describe the position of the chessboard pattern relative to the camera in each image. After the intrinsic and extrinsic matrices were estimated, the corresponding equations were solved to determine the distortion parameters.

After the process of camera calibration, the center point of the chip, focal length (f) and five distortion parameters were known values for us. Two different focal lengths, f_x in the horizontal direction and f_y in the vertical direction, were measured, respectively, but f_x was equal to f_y in our case.

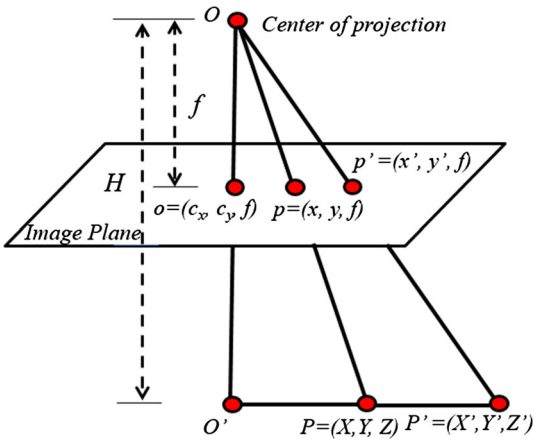

Fig. 2 The relationship between the pixel units and physical units

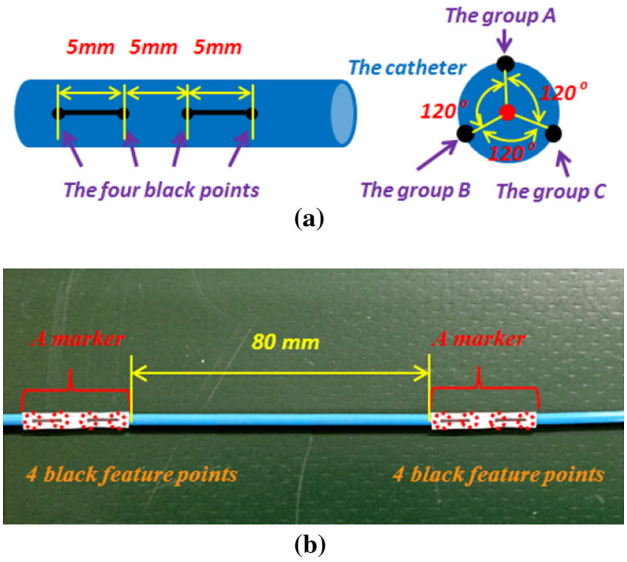

Fig. 3 The markers attached to a 2-mm-diameter catheter. **a** The distribution of a marker: every two black feature points have a 5 mm spacing. **b** The markers attached to a real catheter: every two markers deployed have an 8 cm spacing

The focal length f was actually the combination of the physical focal length of the lens (units of pixels per millimeter) and the size of the individual imager elements (units of millimeters). Distortion parameters were employed to compute a distortion map that was then used to correct the image. The coordinate values of the detected feature points were transformed from their original coordinates to the corresponding undistorted coordinates based on the distortion map. Assuming that point P and P' are two feature points attached to a catheter (shown in Fig. 2), the real distance can be measured as $D_{PP'}$. The two feature points were then detected in the image captured by the camera. The distance in pixels between point p and point p' was marked as $d_{pp'}$. H is the vertical distance between the center of projection and the line PP' and can be calculated based on the principle of similar triangles as:

$$\frac{d_{pp'}}{D_{PP'}} = \frac{d_{\mathrm{Op}}}{D_{\mathrm{OP}}} = \frac{f}{H} => H = \frac{fD_{PP'}}{d_{pp'}} \tag{1}$$

$D_{PP'}$ and f were measurable values. The distance $d_{pp'}$ was computed using $\sqrt{(x'-x)^2+(y'-y)^2}$. D_{OP} and d_{Op} denote the lengths of line OP and line Op, respectively.

After the calculation for height H, the relationship between pixel units and millimeter units was built. A distance in image coordinate system (d_{pixel}) can be transformed to a physical distance (d_{mm}) in millimeters and calculated as:

$$\frac{f}{H} = \frac{d_{\mathrm{pixel}}}{d_{\mathrm{mm}}} => d_{\mathrm{mm}} = \frac{Hd_{\mathrm{pixel}}}{f} \tag{2}$$

To shorten the feature detection time and make it easier to compute the translational displacement and rotational angles of the input catheter, several instrument markers were attached to the catheter. We defined the four feature points (black points) as a group and each instrument marker consisted of three groups (group A, B and C). Every two markers deployed had an 8 cm spacing, and every two black feature points deployed in a marker had a 5 mm spacing. The specific marker distribution is shown in Fig. 3. Note that the markers were extremely thin, and therefore did not enlarge the diameter of the real catheter.

To determine the position of the input catheter, we first needed to extract the markers attached to the catheter. Nineteen best corners with large variation in intensity in all the directions were detected based on the Shi-Tomasi method for detecting corners in a picture captured by the camera. Due to the moving range of the catheter in the camera's view being merely in the middle section, a mask area was used to specify the region in which the corners were detected. The original image was first converted into a grayscale image and then maximized (3) to find the difference in intensity for a displacement of (u, v) in all directions in the specified region:

$$E(u,v) = \sum_{x,y} \omega(x,y)\left[I(x+u, y+v) - I(x,y)\right]^2 \tag{3}$$

where $\omega(x, y)$ is a window function and $I(x+u, y+v)$ denotes shifted intensity and $I(x, y)$ presents intensity.

To achieve better accuracy, sub-pixel level positions of the feature points were computed by interpolating the brightness intensity between the pixels. First, the feature points in pixel accuracy were detected according to the equation above. Then, a small window surrounding the detected position of the feature point was introduced to define the brightness intensity values between pixels using interpolation. We defined step 0.1 pixels between original pixels in which case 1 pixel contains 10 sub-pixels. We can therefore achieve 10

times higher accuracy using sub-pixel level detection. For each feature point q in pixel accuracy, every vector from point q to a point p located surrounding q was orthogonal to the image gradient at p subject to measurement and image noise. The sum of the errors S for point q was defined as:

$$S = \sum_i \nabla H_i^T \cdot (q - p_i) \tag{4}$$

where ∇H_i^T is an image gradient at one of the points p_i in a neighborhood of q, and the iterative algorithm was employed to find the sub-pixel position where S had the minimum value.

After applying the feature detection algorithm, nineteen strongest corners in the specified region were captured, in which four black points in a marker were the desired feature points and the other fifteen points were defined as noise that should be removed. We achieved this purpose based on the distribution rules of the four black points that every two black points deployed in a marker had a 5 mm spacing and four black points in a marker had almost equal coordinate values in the y direction.

The origin of the image was defined at the upper left and the average values of the difference between the four black points in the previous frame, and the current frame in the x and y directions were calculated as the horizontal and vertical displacement of a marker, respectively:

$$\begin{aligned} d_x^{\text{pixel}} &= \left(\sum_{i=1}^{4} \left(X_{\text{cur}}^i - X_{\text{pre}}^i\right)\right) \Big/ 4 \\ d_y^{\text{pixel}} &= \left(\sum_{i=1}^{4} \left(Y_{\text{cur}}^i - Y_{\text{pre}}^i\right)\right) \Big/ 4 \end{aligned} \tag{5}$$

where X_{cur}^i and X_{pre}^i present the pixel coordinates of a black point i in the x direction in the current frame and in the previous frame, respectively. Y_{cur}^i and Y_{pre}^i present the pixel coordinates of a black point i in the y direction in the current frame and in the previous frame, respectively. Additionally, the translational displacement (d_x^{mm}) and rotational angles (θ°) of a catheter were computed as:

$$d_x^{\text{mm}} = d_x^{\text{pixel}} \cdot \frac{f}{H} \tag{6}$$

$$\theta^\circ = \frac{180 \cdot f}{H \cdot \pi \cdot r} \cdot \sigma \cdot d_y^{\text{pixel}} \tag{7}$$

where r is the radius of the catheter and σ is a compensation coefficient for the calculation of rotational angles. Accuracy loss is unavoidable using a line segment ($d_y^{\text{pixel}} \cdot \frac{f}{H}$) to approximate the arc length. We therefore introduced a compensation coefficient σ to make the approximate values close to the true values. σ was defined as the quotient of arc length divided by the corresponding line segment in 120°.

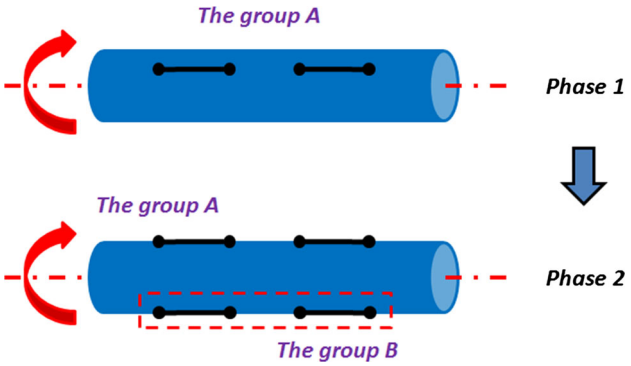

Fig. 4 The critical situation for the rotational motion measurement

As for the proposed detection method, only one group of feature points can appear and be detected in the image at a certain time except the critical situation that is shown in Fig. 4 (Phase 2). In this critical situation, two groups can be detected, and we gave the priority to the group with much higher Y-coordinate value. Thus, the group B in Fig. 4 (Phase 2) was detected. Additionally, the compensation method was triggered in the critical situation. Assuming that the group A was going to reach its travel limit [shown in Fig. 4 (Phase 1)] and two groups (A and B) were found in the critical situation, group B was detected and large variation of Y-coordinate values (the Y-coordinate value of group B is much larger than that of group A) triggered the compensation method. The proposed detection method has the ability to record the Y-coordinate variation values of group A in previous frame and the frame before last. The average value of two Y-coordinate variation values of group A were compensated to the measured rotational angles.

Design of the force feedback unit

Compared to an open surgery, endovascular catheterization techniques have unavoidably reduced the sense of touch leading interventionalists to depend more on the force feedback from catheter–tissue interactions. Although the existing vascular imaging techniques can provide interventionalists with real-time visual feedback about the interactions between the catheter and the patient's vascular structure, haptic feeling is still an important part for the success of endovascular interventional procedures.

The proposed force feedback unit (shown in Fig. 5a, b) consists of a copper coil plate fixed on a bearing holder connected to a slider, a shell with four permanent magnets inside anchored on the movement stage of a screw bearing actuated by a stepper motor, and a bearing with a grasper. An exploded view of the coil plate and its permanent magnet assemblies is shown in Fig. 5c.

The bearing with a grasper (shown in Fig. 6) was used to clamp the catheter. The catheter passed through the bearing

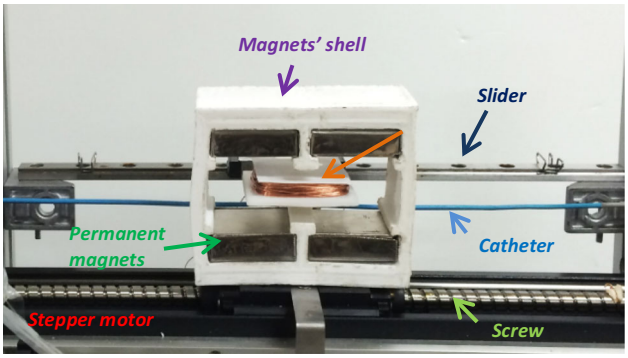

(a)

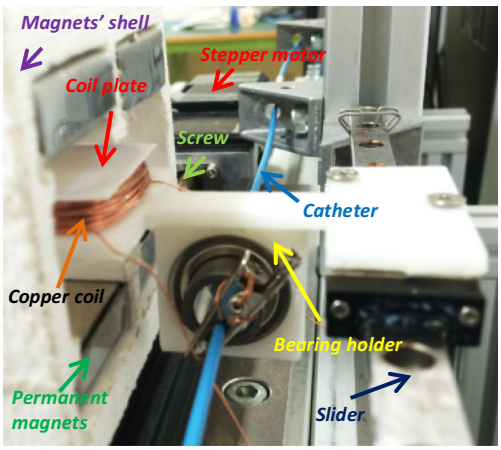

(b)

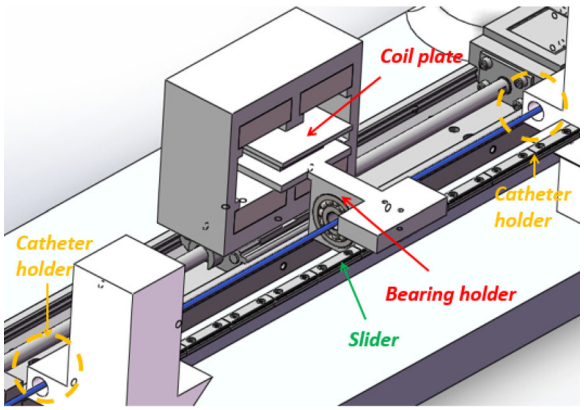

(c)

Fig. 5 The design of the force feedback unit. **a** The front view of the force feedback unit. **b** The lateral view of the force feedback unit. **c** The structure of the force feedback unit

and was integrated with the bearing holder by the grasper. The grasping force integrated the catheter and the bearing together without impairing the catheter because a sponge cushion is applied to the inner surface of the grasper. Thus, the grasping force is small but the friction between the sponge cushion and catheter is strong enough to make them together. The purpose of the design is to not have interference between the two degrees of freedom, namely the design ensures that the axial movements and force feedback do not affect the radial motions and torque feedback.

A hand-wound copper coil was sandwiched between two sheets of plastic board, and the coil plate was incorporated with the catheter by the grasper as the actuator that provides force feedback for the interventionalists. The plastic magnets' shell, produced by a 3D printer, anchored two permanent magnets above the coil. In the same way, the other two matching permanent magnets were anchored below the coil plate. When the prototype was assembled, the distance between the upper and lower magnets was set to 20 mm with the 10-mm-thick coil plate situated in the middle of the gap.

When the coil was energized by a coil current I, it generated a force between the powered coil and the magnetic field B given by:

$$F = -I \int_C B \times \mathrm{d}l \tag{8}$$

where dl is the differential element of wire in the coil, and the integration was calculated over the whole wire between the two pairs of the magnets. The four permanent magnets have powerful magnetic field intensities, thus the magnetic field B is approximately constant between the two pairs of magnets. The generated force by the interaction between the electrified coil and the magnetic field acted linearly along the slider with its orientation decided by the direction of the current. The measured resistance of the coil was 2 Ω. The force resolution was approximately 25 mN and a maximum current of 3A generated an approximately 1.5 N force.

Additionally, lubricants were first used on the catheter holders to decrease frictional resistance. A load cell (TU-UJ, TEAC Corp., Japan) fixed on the movement stage of a screw bearing actuated by a stepper motor was then introduced to measure the friction between catheter and the holders and the slider's friction. The load cell has contact with the slider, and the movement stage is controlled to push and pull the slider to measure the friction. When there is no force feedback to the haptic unit, the coil was powered by the DSP controller to produce an initial force that has the same magnitude but in the opposite direction with the slider's friction so that the pull and push feels frictionless.

Control system mechanisms

Control of the new master controller was achieved by a computer console and a DSP unit (shown in Fig. 7). The DSP unit communicated with the computer console via a RS-232 serial port.

Control software was implemented in C++ to enable simultaneous motion measurements in the axial and radial

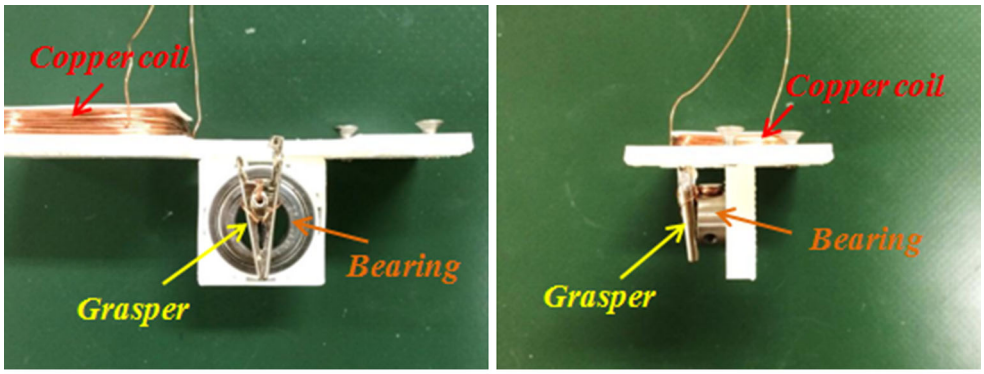

Fig. 6 The design of the bearing with a grasper. **a** A front view. **b** A lateral view

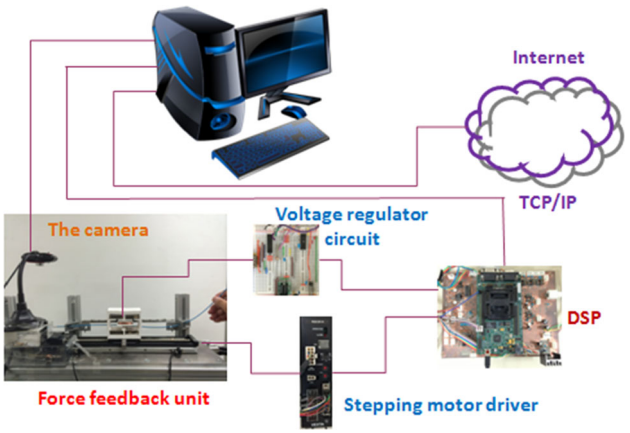

Fig. 7 The schematic of the control system

directions. The axial position of the input catheter was transmitted to the DSP unit through the RS-232 serial port. To prolong the operation range, the magnet's shell followed the motion of the coil plate to provide a magnetic field. A PID control loop implemented on the DSP unit was employed to control the relative position between the magnets' shell and the coil plate running at 1000 Hz, namely the PID control loop aims to maintain a zero offset between the movement stage and the catheter. The encoder measured the position of the movement stage so that the difference between the translational displacement and the measured displacement of the catheter forms the input to the PID controller. To output a stable voltage to the coil, a voltage regulator circuit was designed to control the current of the force feedback device by the DSP unit. The refresh rate was 1000 Hz which is a commonly accepted refresh rate to provide realistic force feedback [28].

Additionally, the control software implemented on the computer is able to control the simulated catheter in a virtual reality training system or to drive a slave manipulator in the axial and radial motion based on the Internet.

Experimental results

To demonstrate the performance of the catheter-sensing unit and the force feedback unit, the proposed master controller was evaluated with a series of experiments.

Evaluation of the feature extraction algorithm

According to the feature extraction algorithm based on (3) and (4), the results of the method are shown in Figs. 8 and 9. We first detected the nineteen corner points with a large variation in intensity in the mask region. The noise points were then removed based on the distribution rules of the four black points. The average displacement of the four feature points of group A, group B or group C in x direction was used to determine the axial motion of the catheter based on (6). For the radial motion, the average displacement of the four feature points of group A in the y direction was applied to compute the rotational angles of the catheter based on (7). When group A reached its travel limit, group B was then detected to measure the radial motion of the catheter instead of group A. The measurement range of the rotational angles for each group was 120°.

Evaluation of the catheter-sensing unit

To evaluate the performance of the catheter-sensing unit, we used a stepper motor (VEXTA ASM46AA, resolution 1000P/R) with an encoder (1000 count-per-revolution quadrature encoder) to pull, push and rotate the catheter and compared the data obtained by the encoder with translational and rotational results computed by the catheter-sensing unit. Insertion and extraction was conducted at an approximately constant velocity of 8.4 mm/s. From the experimental results, 288 frames were captured by the camera and only one frame was failed to detect the feature points. The error frame would not damage the measurement results because only the

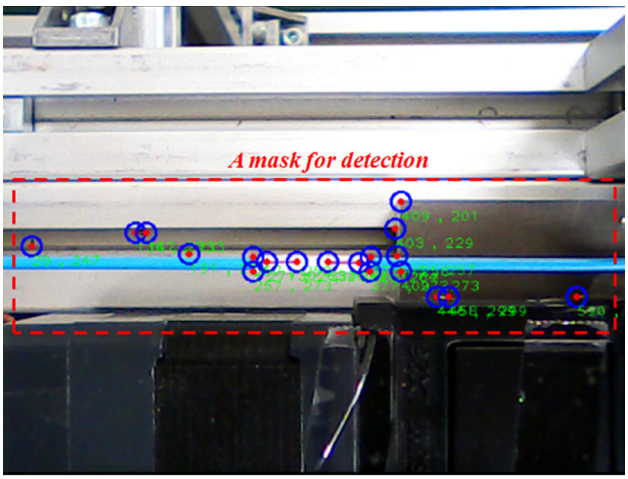

(a)

(b)

Fig. 8 The results of the feature detection algorithm. **a** The strongest corners detection. **b** 4-Feature-point detection

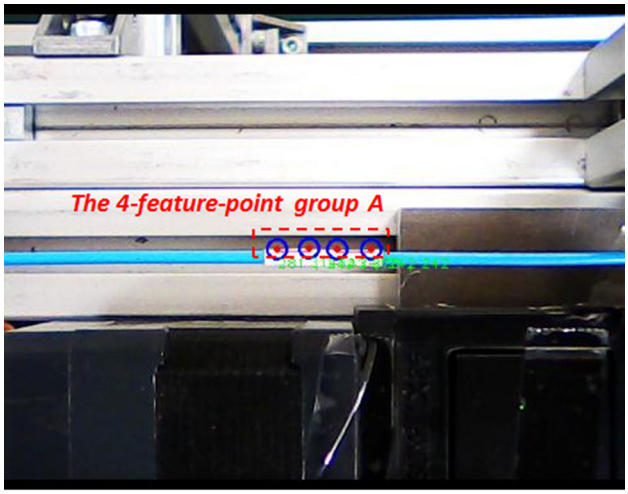

(a)

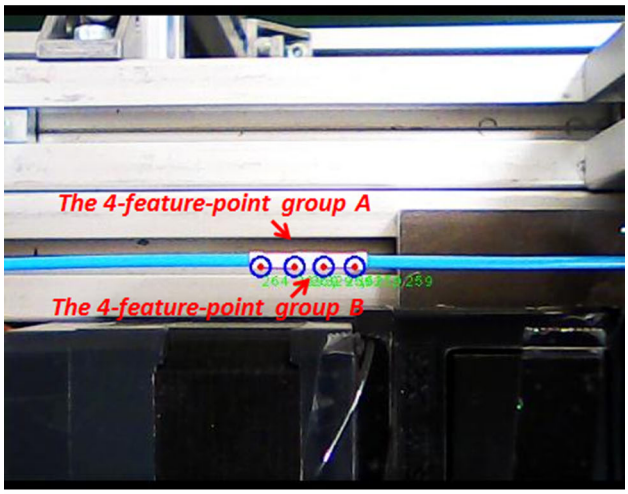

(b)

Fig. 9 The process of capturing feature points for the rotational calculation. **a** The top position of the 4-feature-point group A. **b** The bottom position of the 4-feature-point group B

variation of displacement contributed to the detected displacement. The rotation was performed at an approximately constant angular velocity of 115°/s. From the experimental results, 52 frames were captured by the camera with 100% success rate for the feature points' detection. The data obtained from the encoder were used as the benchmark. The comparative results of insertion/extraction and rotation motions are shown in Figs. 10 and 11, respectively.

Additionally, another 20 groups of insertion and extraction experiments were performed. The results of insertion/extraction experiments with the same displacement (40 mm) at different velocities are shown in Fig. 12. The comparative results with the same velocity (33.6 mm/s) in different displacements are shown in Fig. 13. Other experimental results for the radial motion of the catheter between the encoder and the catheter-sensing unit are shown in Fig. 14. The measurement range of each marker for rotational angles was 0°–120°. From the experimental results, the minimum and the maximum errors of translational displacement were 0.003 mm (0.01%) and 0.425 mm (1.06%), respectively. The average error was 0.113 mm (0.28%). In terms of rotational angles, the minimum and the maximum error were 0.39° (0.325%) and 7.2° (6%), respectively. The average error was 3.61° (3.01%).

Evaluation of force feedback unit

To provide the force feedback based on a magnetic force generated by the permanent magnets and the powered coil, the first step was to build a relationship between the current and the magnetic force. We used a load cell, shown in Fig. 15, to measure the force generated by the force feedback unit. A

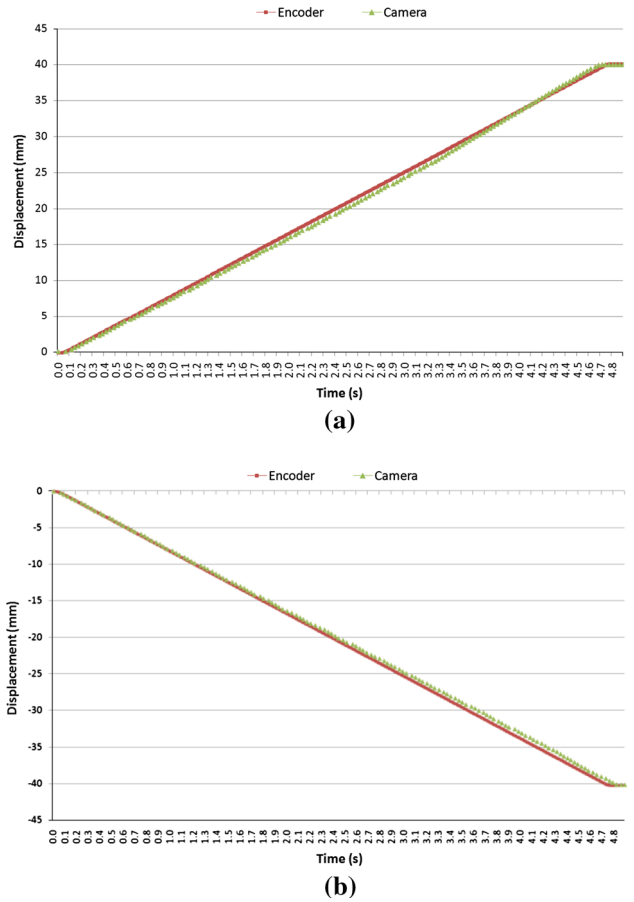

Fig. 10 The results of the insertion and extraction motion. **a** The insertion motion. **b** The extraction motion

regulated DC power supply was then introduced to provide the excitation current to the coil gradually increasing from 0 to 1.08 A by increments of 0.01 A. A trend line was defined as the relationship between the current and the force shown in Fig. 16. It was almost a linear relationship with the fitted linear equation:

$$y = 0.5817x - 0.071 \tag{9}$$

where y presents the force and x is the input current. Due to the slider's friction, the initial current was set to 0.14 A.

When the force measured by the slave system (catheter-manipulating device located in the patient's site) was transmitted back to the master controller, the current can be computed according to the force based on (9). Assuming that the force measured by the slave system (blue curve in Fig. 17) was transmitted to the master controller, the force feedback unit controlled the current to generate the corresponding magnetic force based on the relationship between the current and the magnetic force. In order to evaluate the performance of the force feedback unit,

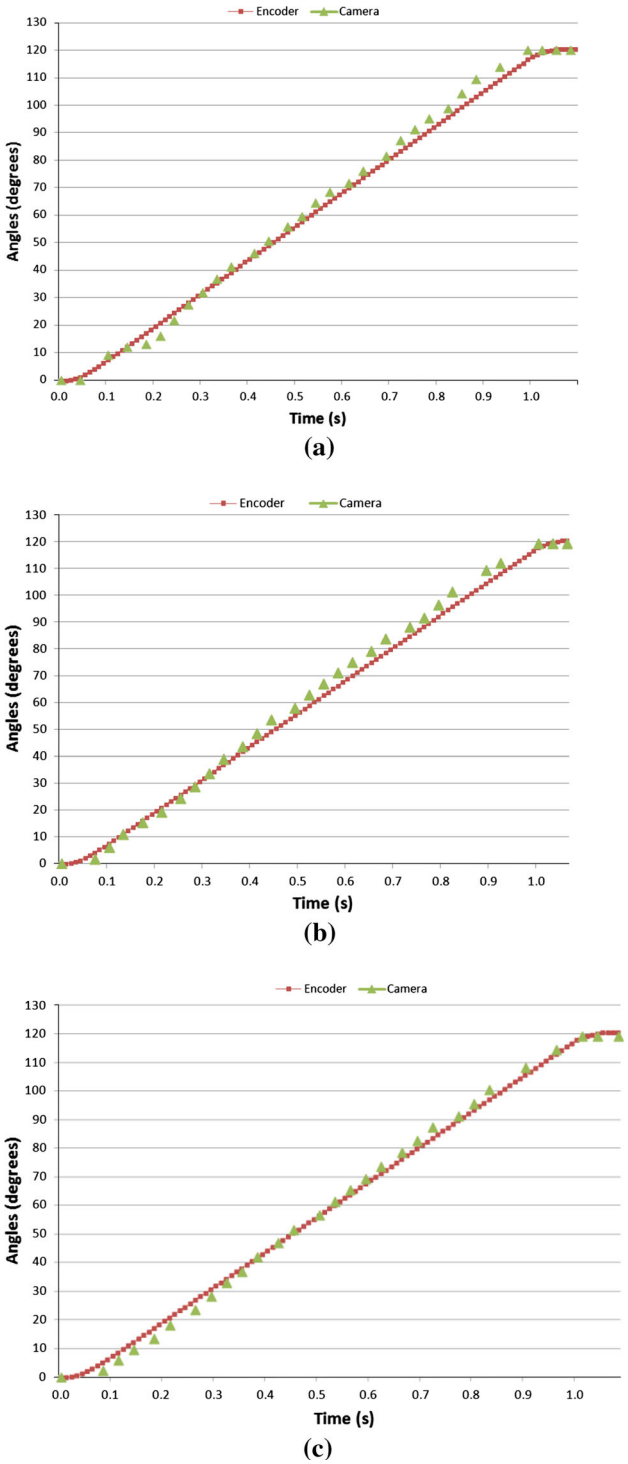

Fig. 11 The results of the rotation motion. **a** The 4-feature-point group A. **b** The 4-feature-point group B. **c** The 4-feature-point group C

a load cell was employed to measure the force generated by the powered coil and the magnetic field. The results are shown by the red curve in Fig. 17. The minimum error was 0.0052 N and the maximum error was 0.0247 N.

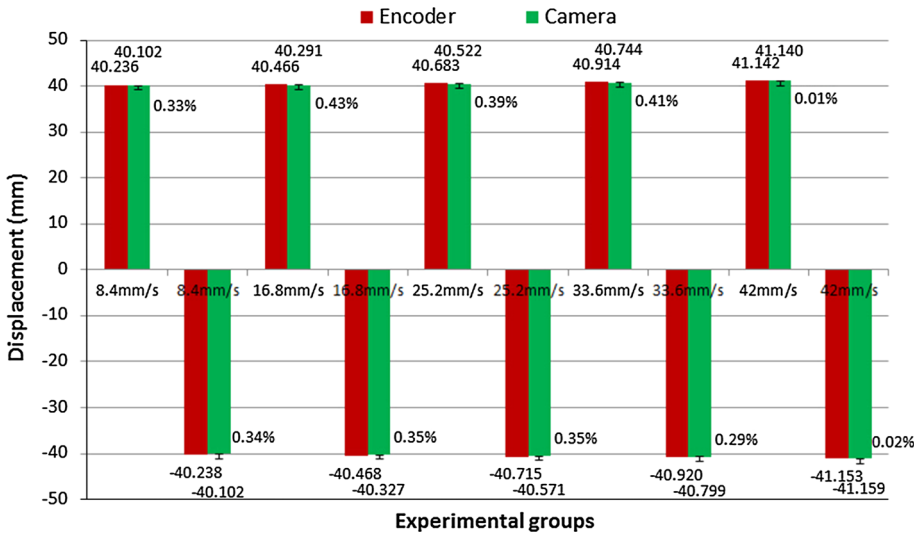

Fig. 12 The results of pull/push experiments with different velocities

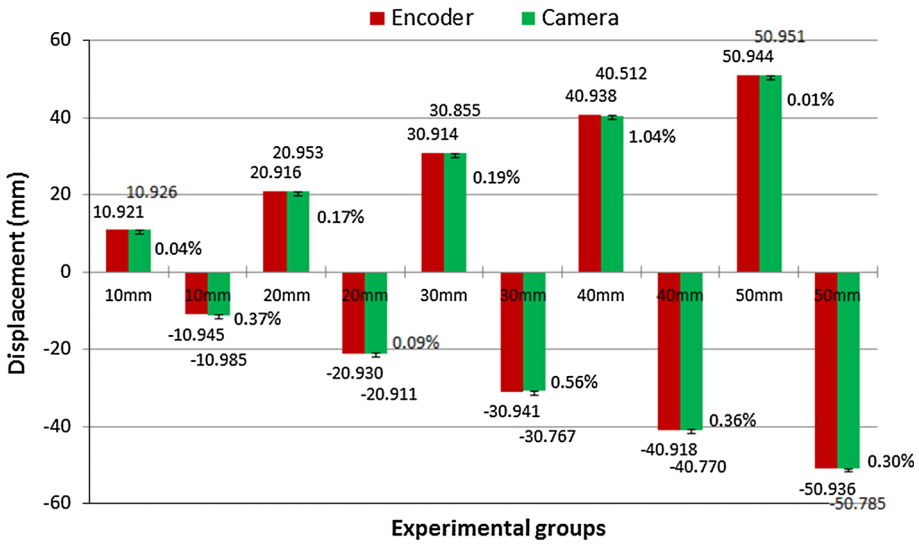

Fig. 13 The results of pull/push experiments with different displacements

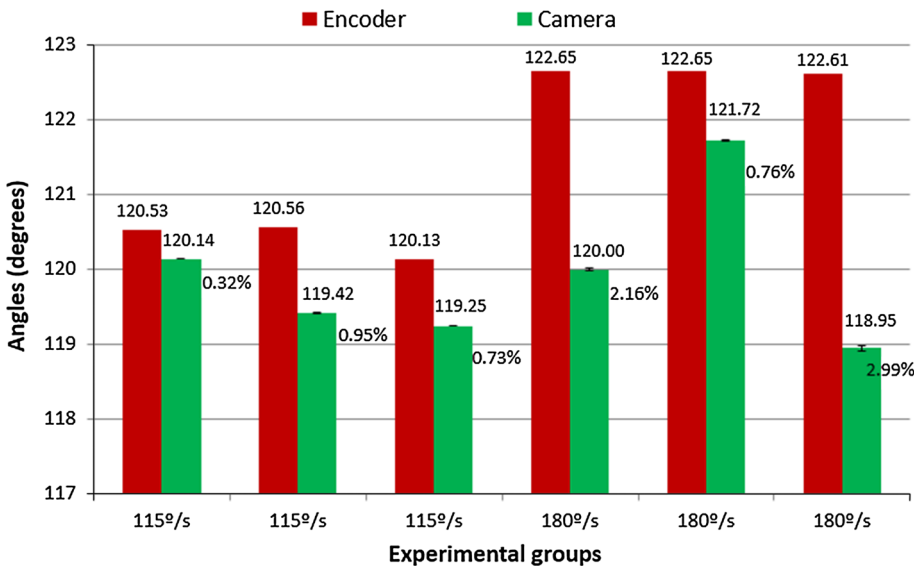

Fig. 14 The results of the rotation experiments with different velocities

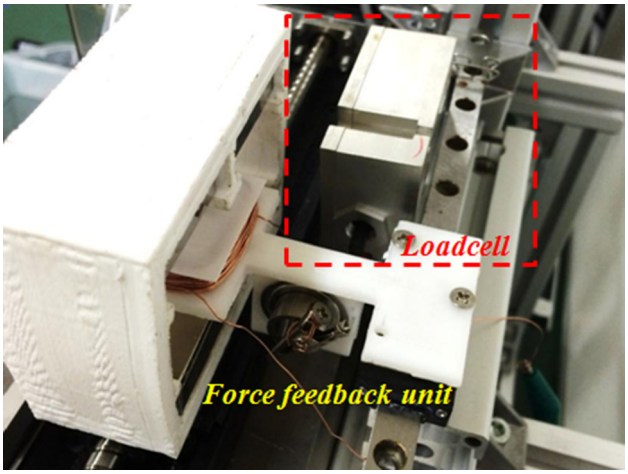

Fig. 15 The experimental setup for the evaluation of the force feedback unit

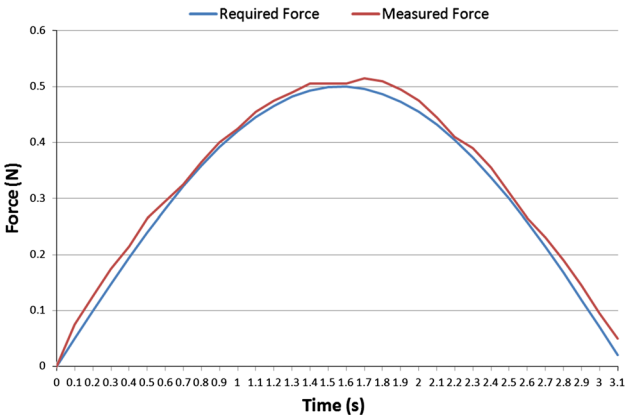

Fig. 17 The comparative results between the require force and the measured force

Discussion

Compared to previous designs, the proposed master controller allowed a contactless measurement, which avoids additional friction and provided contactless force feedback in the axial direction to interventionalists. Moreover, the design enforced the catheter straight below the camera regardless of how they push, pull or twist the catheter. The interventionalists can manipulate the catheter according to their own habits. It is applicable not only to catheterization but also to other similar interventions. The current implementation of the master controller is designed for use with 6–7 F catheters, and the design can be easily adapted for catheters of larger sizes. However, utilizing this design with smaller catheters will require modifying the markers attached to the catheter. A short hollow cylinder with a larger size can be used to load the markers below the camera. The catheter passing through the hollow cylinder can rotate coaxially with the hollow cylinder. The marking method and the image processing algorithms are the same with the proposed catheter-sensing unit. The proposed master controller has many potential advantages over commercially available systems. Unlike most commercial catheterization training systems utilizing joystick-type input devices or specialized catheters to navigate the slave manipulator or simulated catheter in VR systems, the proposed master controller has the ability to use actual and generic catheters. Additionally, the proposed master controller has a simple and compact structure and is more cost-effective that also allows conventional pushing, pulling and twisting of the catheter during the catheterization procedure. Researchers in [15] have pointed out that robotic surgery based on the commercially available system is too expensive. The systems are costly over 600,000 dollars with high maintenance costs of approximately 60,000 dollars to 80,000 dollars. Additional cost is that of disposable high-tech catheters, which are again expensive; the Hansen catheter costing upwards of 1500 dollars. For the simulator training, the best or most realistic simulators may cost up to 500,000 dollars which is not widely available [29].

Fig. 16 The calibration results between the current and the force

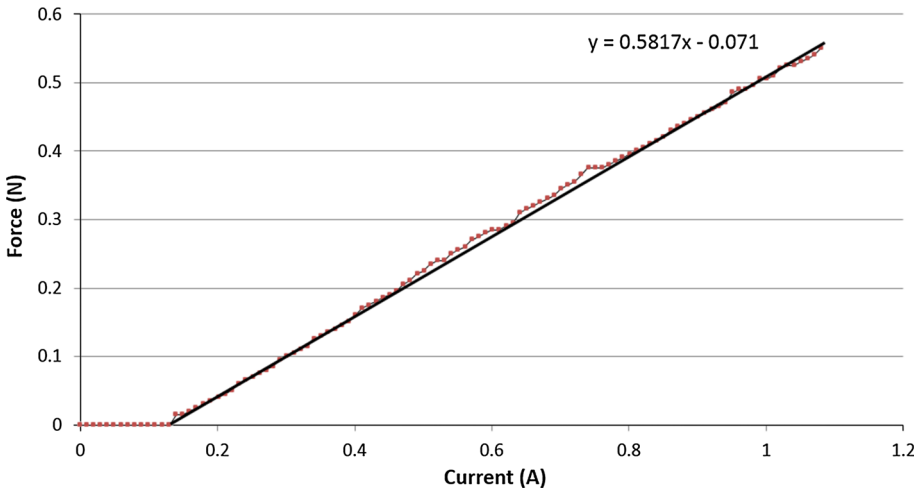

The new master controller described in this paper was designed to operate in two modes: (1) It can be employed as a controller to enable interventionalists to use their highly developed dexterous skills to remotely maneuver the slave catheter manipulator, potentially reducing radiation exposure and physical stress during long procedures. The slave system can connect to the master controller based on Internet for remote experiments over inter-country distances or a cable for short distance operations. The resultant force at the proximal end of the catheter resulting from catheter–tissue interactions sensed by the slave system can exert on the catheter of the new master controller to provide operators with a sense of resistance. (2) It can be used to pull, push or twist the simulated catheter in a virtual reality-based training system. VR-based simulators offer flexible scenarios with a high degree of realism. Interventionalists can create any desired scenario according to the corresponding computerized tomography (CT) or magnetic resonance imaging (MRI) dataset. Additionally, the elastic characteristic can be set to simulate different kinds of soft tissues. The interaction force between the simulated catheter and its surrounding virtual vascular structure can be provided to the operators' hands via the force feedback unit of the proposed master controller.

Conclusion and future work

Based on analysis of requirements and state-of-the-art computer-assisted and robot-assisted training systems for endovascular catheterization, a new master controller with a force feedback interface was proposed to maintain natural endovascular catheterization skills of interventionalists. A camera was employed to simultaneously detect the axial and radial motions of the catheter with the ability to allow interventionalists to use their dexterous skills while performing catheter-based interventions. Additionally, a force feedback unit was developed to provide the operators with a sense of resistance force. A series of experiments were carried out to evaluate the performance of the catheter-sensing unit and the force feedback unit.

The proposed master controller in this paper has no function of rotational force feedback. Thus, future work includes the development of a rotational force feedback unit to provide the interventionalists with a resistance feeling in the radial direction.

Acknowledgments This research was supported partly by National High Tech. Research and Development Program of China (No. 2015AA043202) and the Kagawa University Characteristic Prior Research Fund 2012.

Conflict of interest The authors have stated explicitly that there are no conflicts of interest in connection with this article.

References

1. Guiatni M, Riboulet V, Duriez C, Kheddar A, Cotin S (2013) A combined force and thermal feedback interface for minimally invasive procedures simulation. IEEE/ASME Trans Mechatron 18(3):1170–1181
2. Wang J, Ohya T, Liao H, Sakuma I, Wang T, Tohnai I, Iwai T (2011) Intravascular catheter navigation using path planning and virtual visual feedback for oral cancer treatment. Int J Med Robot Comput Assist Surg 7:214–224
3. Luan K, Ohya T, Liao H, Kobayashi E, Sakuma I (2013) Vessel bifurcation localization based on intraoperative three-dimensional ultrasound and catheter path for image-guided catheter intervention of oral cancers. Comput Med Imaging Graph 37(2):113–122
4. Srimathveeravalli G, Kesavadas T, Li X (2010) Design and fabrication of a robotic mechanism for remote steering and positioning of interventional devices. Int J Med Robot Comput Assist Surg 6:160–170
5. http://www.mentice.com/our-simulators/
6. Aggarwal R, Black SA, Hance JR, Darzi A, Cheshire NJW (2006) Virtual reality simulation training can improve inexperienced surgeons' endovascular skills. Eur J Vasc Endovasc Surg 31(6):588–593
7. http://simbionix.com/simulators/angio-mentor/
8. Eslahpazir BA, Goldstone J, Allemang MT, Wang JC, Kashyap VS (2014) Principal considerations for the contemporary high-fidelity endovascular simulator design used in training and evaluation. J Vasc Surg 59(4):1154–1162
9. Desser TS (2007) Simulation-based training: the next revolution in radiology education? J Am Coll Radiol 4(11):816–824
10. http://www.hansenmedical.com/int/en/vascular/magellan-robotic-system/product-overview
11. Saliba W, Reddy VY, Wazni O, Cummings JE, David Burkhardt J, Haissaguerre M, Kautzner J, Peichl P, Neuzil P, Schibgilla V, Noelker G, Brachmann J, Di Biase L, Barrett C, Jais P, Natale A (2008) Atrial fibrillation ablation using a robotic catheter remote control system. J Am Coll Cardiol 51(25):2407–2411
12. http://www.stereotaxis.com/index.php
13. Chun KRJ, Schmidt B, Köktürk B, Tilz R, Fürnkranz A, Konstantinidou M, Wissner E, Metzner A, Ouyang F, Kuck K-H (2008) Catheter ablation—new developments in robotics. Herz 33:586–589
14. Payne, CJ, Rafii-Tari H, Yang G-Z (2012) A force feedback system for endovascular catheterisation. In: Proceedings of the IEEE/RSJ international conference on intelligent robots and systems, pp 1298–1304, October 7–12, Vilamoura, Algarve, Portugal
15. Antoniou GA, Riga CV, Mayer EK, Cheshire NJW, Bicknell CD (2011) Clinical applications of robotic technology in vascular and endovascular surgery. J Vasc Surg 53(2):493–499
16. Das P, Goyal T, Xue A, Kalatoor S, Guillaume D (2014) Simulation training in neurological surgery. Austin J Neurosurg 1(1):1–6
17. Binning MJ, Siddiqui AH, Levy EI, Hopkins LN (2012) Avoiding complications during percutaneous cardiovascular interventions: What should we learn from the aviation industry? In: Complications of interventional cardiovascular procedures: a case-based Atlas. Demos Medical Publishing, pp 1–7
18. Cercenelli L, Marcelli E, Plicchi G (2007) Initial experience with a telerobotic system to remotely navigate and automatically reposition standard steerable EP catheters. Am Soc Artif Intern Organs J 53(5):523–529
19. Marcelli E, Cercenelli L, Plicchi G (2008) A novel telerobotic system to remotely navigate standard electrophysiology catheters. In: Computers in cardiology, 2008, September 14–17, Bologna, Italy, pp 137–140

20. Tanimoto M, Arai F, Fukuda T, Iwata H, Itoigawa K, Gotoh Y, Hashimoto M, Negoro M (1997) Micro force sensor for intravascular neurosurgery. In: Proceedings of the IEEE international conference on robotics and automation, April 20–25, Albuquerque, NM, pp 1561–1566
21. Negoro M, Tanimoto M, Arai F, Fukuda T, Fukasaku K, Takahashi I, Miyachi S (2002) An intelligent catheter system robotic controlled catheter system. Interv Neuroradiol 7:111–113
22. Tercero C, Ikeda S, Fukuda T, Arai F, Negoro M, Takahashi I (2010) Numerical comparison of catheter insertion trajectory within blood vessel model using image processing. In: 2010 international symposium on micro-nanomechatronics and human science, November 7–10, Nagoya, Japan, pp 378–383
23. Guo J, Guo S, Xiao N, Ma X, Yoshida S, Takashi T, Masahiko K (2012) A novel robotic catheter system with force and visual feedback for vascular interventional surgery. Int J Mechatron Autom 2(1):15–24
24. Thakui Y, Bax JS, Holdsworth DW, Drangova M (2009) Design and performance evaluation of a remote catheter navigation system. IEEE Trans Biomed Eng 56(7):1901–1908
25. Ma X, Guo S, Xiao N, Yoshida S, Tamiya T (2013) Evaluating performance of a novel developed robotic catheter manipulating system. J Micro-Bio Robot 8(3–4):133–143
26. Kaehler A, Bradski G (2008) Learning OpenCV. O'Reilly Media, Sebastopol
27. Zhang Z (2002) A flexible new technique for camera calibration. IEEE Trans Pattern Anal Mach Intell 22(11):1330–1334
28. Coles TR, Meglan D, John NW (2011) The role of haptics in medical training simulators: a survey of the state of the art. IEEE Trans Haptics 4(1):51–66
29. Moussa I, Bailey S, Colombo A (2012) Complications of interventional cardiovascular procedures: a case-based atlas. Demos Medical, New York